ChemPubSoc Europe

DOI: 10.1002/cphc.201402002

Far-Red Organic Fluorophores Contain a Fluorescent Impurity

Matthew B. Stone and Sarah L. Veatch*[a]

Far-red organic fluorophores commonly used in traditional and super-resolution localization microscopy are found to contain a fluorescent impurity with green excitation and near-red emission. This near-red fluorescent impurity can interfere with some multicolor stochastic optical reconstruction microscopy/photoactivated localization microscopy measurements in live cells and produce subtle artifacts in chemically fixed cells. We additionally describe alternatives to avoid artifacts in super-resolution localization microscopy.

The far-red dyes Cy5 and Alexa 647 are popular choices for diverse fluorescence applications because they have large extinction coefficients, high quantum yields, and excitation maxima at frequencies with low cellular absorption. These dyes and their structural analogs are a preferred choice for (direct) stochastic optical reconstruction microscopy [(d)STORM] because they exhibit highly favorable photoswitching characteristics,[1–4] allowing densely labeled proteins to be stochastically sampled and localized as single molecules. It is possible to conduct quantitative, two-color super-resolution experiments by imaging a far-red photoswitchable organic dye together with a spectrally distinct organic dye or fluorescent protein.[5–10] Two-color super-resolution experiments reveal the nanoscale locations of two independently-labeled sets of biomolecules, allowing quantitative analysis of co-clustering, oligomerization, and relative diffusion.[11–14]

Here, we describe a fluorescent anomaly associated with Cy5, Alexa 647 and structurally related dyes that can interfere with quantitative two-color super-resolution measurements. This anomaly is demonstrated in Figure 1a where endogenous B cell receptor (BCR) is labeled with f(Ab)$_1$ conjugated to either Alexa 647 or Cy5. Live CH27 cells are simultaneously illuminated with both 640 nm and 561 nm lasers under total internal reflection while far-red (660 nm–740 nm) and near-red (576–630 nm) emissions are collected. Receptors are detected in the far-red emission channel as expected. Surprisingly, a fluorescent signal is also observed in the near-red emission channel. Fluorescent signals in the near-red emission channel can be observed by viewing raw data (Movie S1), reconstructed super-resolution images (Figure 1a), or by counting the rate of events that occur per unit area (Figure 1b). Here, an event is defined as a local maximum with intensity greater than five times the standard deviation of the noise and is well fit by a defined Gaussian, as detailed in the Experimental Section. A similar population of near-red emitting fluorophores is observed when antibodies are conjugated to reactive fluoro-

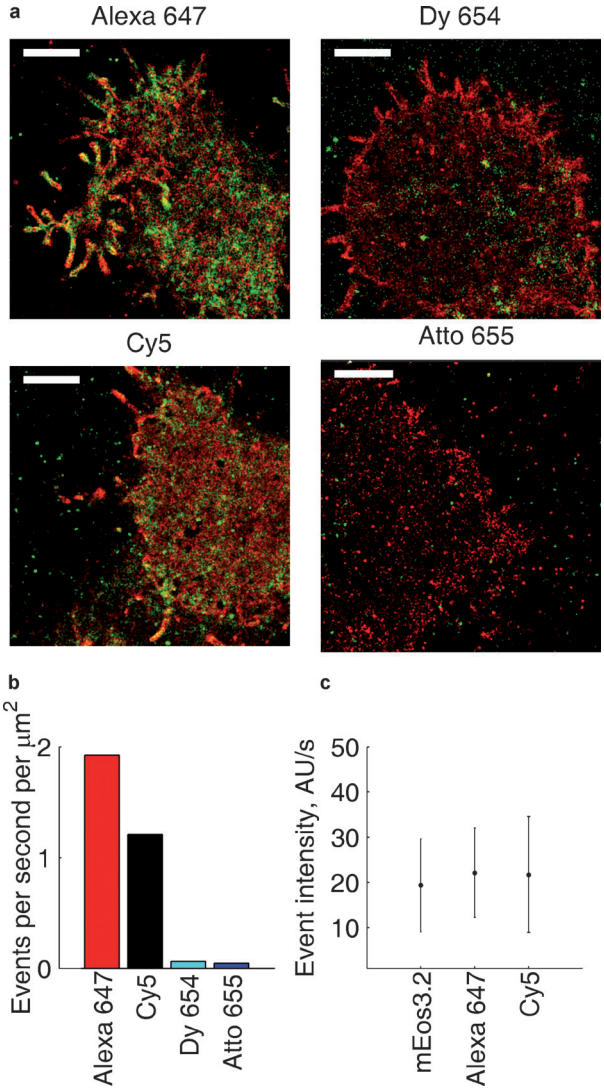

Figure 1. Near- and far-red emission is observed with simultaneous 640 and 561 nm excitation. a) CH27 cells are labeled with f(Ab)$_1$ anti BCR conjugated to the indicated dye and observed through simultaneous illumination with 561 and 640 nm laser light. Emission was separated using a dichroic and bandpass filter set, and reconstructed images of near-red emission (576630 nm) are shown in green and far-red emission (660–740 nm) shown in red. Scale bars are 3 μm. b) The number of events per second per μm^2 detected during the simultaneous excitation as bar plots. c) The average event intensity per second for mEos3.2, Alexa 647, and Cy5 excited by 561 nm laser light. Laser intensity and camera settings were kept constant between measurements. Error bars indicate one standard deviation.

[a] *M. B. Stone, Prof. S. L. Veatch*
Department of Biophysics
University of Michigan, 930 N University
Ann Arbor MI 48109 (USA)
E-mail: sveatch@umich.edu

Supporting Information for this article is available on the WWW under http://dx.doi.org/10.1002/cphc.201402002.

phores of different batch numbers, when antibodies are conjugated to fresh reactive dye stocks or stocks that have been stored in dimethyl sulfoxide (DMSO) at −80 °C for >1 year, when antibodies or toxins are purchased pre-conjugated to fluorophores, or when supported membranes are labelled with DiD-C18, a fluorescent lipid analog that is structurally similar to Cy5 (Movie S2 and S3). We performed two-color super-resolution imaging with identical excitation and acquisition conditions to compare the density and intensity of near-red fluorescent events between four different far-red dyes. Endogenous BCR expression levels do not vary dramatically between cells; therefore, the density of events is compared.

The number of events observed in the near-red channel is dramatically reduced when the alternative STORM dyes Dyomics 654 and Atto 655 are used (Figure 1 and Movie S4). The intensities of near-red fluorescent events from Alexa 647 and Cy5 are comparable to those of mEos3.2[15,16] when either fluorophore is excited by 561 nm light. Near-red fluorescent events from Alexa 647 and Cy5 are also apparent when cells are illuminated with 532 nm light and near-red emission is collected between 545 and 620 nm. Again, fewer fluorescent events are observed in the near-red emission channel when cells are labelled with antibodies conjugated to Dyomics 654 or Atto 655 and excited with 532 nm light (Figure 2a–c). The intensity of near-red fluorescent events from Alexa 647 and Cy5 are comparable to those from Alexa 532 under the same illumination conditions. We find that the density of near-red events does not vary with time over the course of an experiment and do not depend on the presence of 640 nm excitation, suggesting that they are not induced by the laser excitation. Fluorescent events detected in both channels are diffusive under our imaging conditions (Movie S1, S2, and S3) and are not correlated in space. This observation suggests that the fluorescent anomaly is an impurity present in the reactive dye stock with blue-shifted spectral characteristics, and not simply bleed through of fluorescence between channels. We find that this fluorescent moiety does not photoswitch in the presence of the oxygen depleted and reducing imaging buffer, leading to long single-molecule trajectories. This photostability results in a large number of fluorescent events in the near-red emission channel when compared to the far-red emission channel. This occurs even when the relative concentration of the near-red fluorescent moiety is a small fraction of total dye since near-red fluorophores are visible at all times whereas the vast majority of far-red fluorophores are in a reversible dark state.

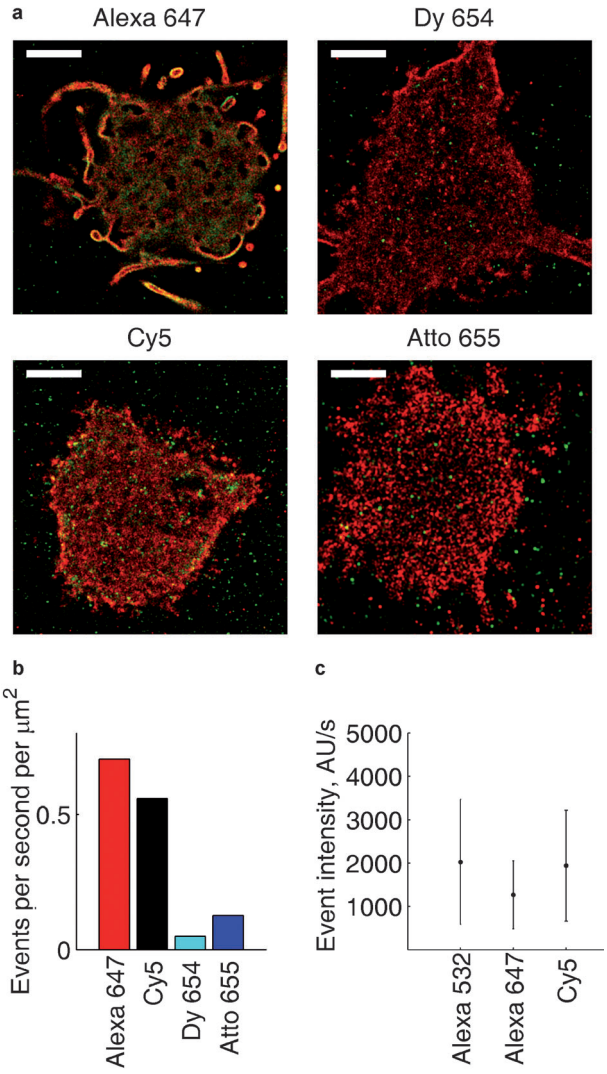

Figure 2. Near- and far-red emission is observed with simultaneous 640 and 532 nm excitation. a) CH27 cells are labeled with $f(Ab)_1$ anti BCR that was conjugated to the indicated dye and observed through simultaneous illumination with 532 and 640 nm laser light. Emission was separated using a dichroic and bandpass filter set, and reconstructed images of near-red emission (545 nm–620 nm) are shown in green and far-red emission (660–740 nm) shown in red. Scale bars are 3 μm. b) The number of events per second per μm^2 detected during the simultaneous excitation as bar plots. c) The average event intensity per second for Alexa 532, Alexa 647, and Cy5 excited by 532 laser light. Laser intensity and camera settings were kept constant between measurements. Error bars indicate one standard deviation.

Near-red fluorescence is also observed in bulk fluorescence assays of Alexa 647 conjugated to antibodies, and in unconjugated Alexa 647 diluted in phosphate buffered saline (PBS, Figure 3a). The 560 nm peak in these emission spectra of Alexa 647 arises from the near-red fluorescent species, while the second peak at 660 nm corresponds to the expected far-red emission maxima of Alexa 647. These spectra confirm that the near-red fluorescent species is present in the reactive dye stock prior to conjugation and is not a consequence of antibody conjugation. This also confirms that the near-red fluorescent species can conjugate to antibodies. The expected Alexa 647 emission peak is of roughly equal magnitude to the near-red emission because these probes are excited far from their excitation maxima, and not because these species are of roughly equal concentration in solution (see below). Unconjugated Cy5 also shows an emission maximum near 560 nm with a similar magnitude to Alexa647 when diluted to the same concentration (1 μM; Figure 3b). In contrast, the emission intensity in this spectral region is greatly reduced for the case of Dyomics 654 and Atto 655, in good agreement with the single-molecule observations shown in Figures 1 and 2. We measured the excitation spectrum of unconjugated Alexa 647 in PBS using emission collection at 575 nm. The shape of the

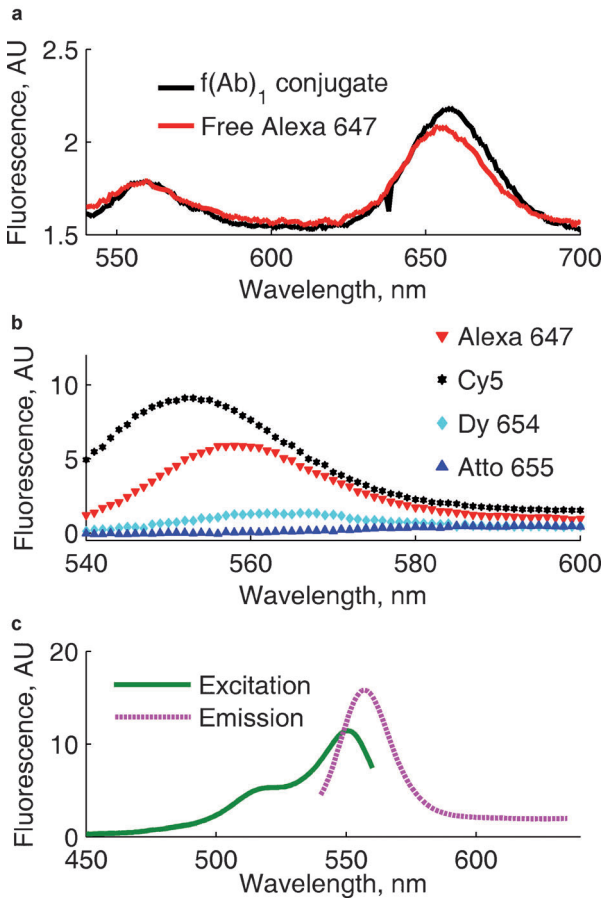

Figure 3. Near-red emission is observed in bulk fluorescence measurements. a) The fluorescence emission spectrum of Alexa 647 either as the unconjugated NHS ester (800 nM) or conjugated to $f(Ab)_1$ (50 $\mu g\,mL^{-1}$). Samples are excited by 530 nm light with identical gain and bandwith. The magnitude of near-red emission and the overall shape of the spectra are comparable between the two samples. b) Fluorescence emission spectra of the four dyes with excitation at 530 nm. All dyes are diluted to 1 μM in PBS and the near-red portion of the spectrum is shown. c) Fluorescence excitation and emission spectra of the near-red moiety in Alexa 647 NHS ester. The excitation spectrum is acquired by monitoring emission at 575 ± 2 nm over a range of excitation wavelengths. The emission spectrum is acquired by exciting at 530 nm. The gain is held constant within but not between each subfigure.

excitation spectrum is similar to other fluorophores with an excitation peak near 550 nm and a shoulder from 520–530 nm (Figure 3c). The near-red emitting species has excitation and emission maxima near 550 nm and 560 nm respectively, which is similar to the Cy3 fluorophore but with a smaller Stokes shift. These bulk fluorescence measurements are consistent with our observations of single-molecule intensities. We find that near-red single-molecule event intensities are roughly two orders of magnitude greater when excited using a Cy3 filter set (ex: 532 nm/Em: 545 nm–620 nm) than when excited with a red fluorescent protein (RFP) filter set (Ex 561 nm/Em 576 nm–630 nm). This occurs because the excitation and emission windows for the Cy3 set are more centered on prominent regions emission and excitation spectra. Unfortunately, the single-molecule intensities of these anomalous near-red events are comparable to those of the common super-resolution probes using both filter sets (Figure 1c and 2c). When excited with 532 nm light, the anomalous near-red single molecule intensities are indistinguishable from Alexa 532 acquired under the same imaging conditions. When excited at 561 nm, the anomalous near-red fluorescence intensity closely resembles that of the commonly used photoactivated localization microscopy (PALM) probe mEos3.2.

Previous work has demonstrated that cyanine dyes can dimerize and aggregate in aqueous solution, changing their absorption and emission spectra.[17] To determine if the observed near-red fluorescence is a result of dye aggregation, we examined the fluorescence and absorbance of unconjugated Alexa 647 NHS ester over a range of dye concentrations. We find that the molar intensity of the near-red emission is weakly quenched at higher dye concentrations (Figure 4a), indicating that the anomalous fluorescence is not a result of aggregation. If this were the case, higher concentrations should increase the fraction of dimers or higher order aggregates. Additionally, we do not detect the emergence of strong H-band absorbance[18,19] at concentrations relevant for dye conjugation to labeling antibodies (Figure 4b), again suggesting that dyes are not aggregating in large quantities.

Finally, we characterize the diffusion and number of near-red and far-red fluorophores of Alexa 647 NHS ester in aqueous dilutions using fluorescence correlation spectroscopy (FCS, Figure 5). From the acquired FCS spectra we extract both the

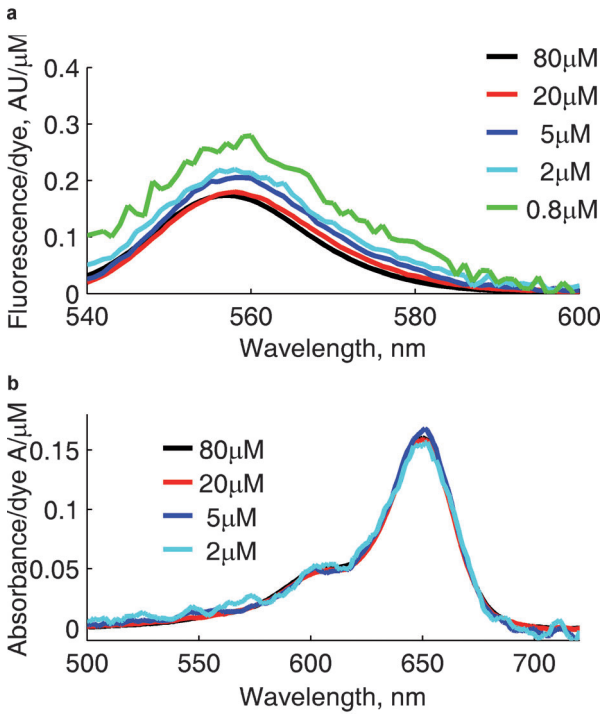

Figure 4. Fluorescence and absorbance spectra are not concentration-dependent. a) Fluorescence emission spectra at 530 nm excitation of unconjugated Alexa 647 NHS ester diluted into PBS at various concentrations. Fluorescence intensity is normalized by the concentration of the dye. b) Absorbance spectra of unconjugated Alexa 647 NHS ester diluted into PBS at various concentrations. Absorbance is normalized by the concentration of the dye.

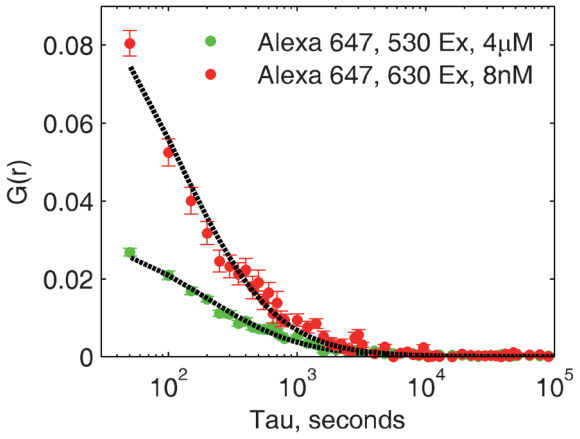

Figure 5. FCS correlation curves for unconjugated Alexa 647. Time correlation curves for Alexa 647 far-red and near-red emission were determined by diluting Alexa 647 to 8 nM and exciting with 630 nm light, or by diluting Alexa 647 to 4 μM and exciting with 530 nm light. Dotted black lines are fits to Equation (1) and are used to extract fit parameters for Table 1.

concentration and diffusion coefficient of both species, as described in the Experimental Section. We find that there is approximately one green fluorescent moiety for every 300 far-red Alexa 647 fluorophores (Table 1) indicating that the fluorescent

Table 1. Concentrations of Alexa 647 determined by FCS.

Excitation	$C_{dilution}$	C_{FCS}	$C_{dilution}/C_{FCS}$
630 nm	8 nM	6 nM	1.1
530 nm	4 μM	12 nM	308

impurity is present at 0.3%, well within the quoted purity of the commercially acquired compound. We additionally observe similar rates of diffusion for the two fluorescence species, 240 $\mu m^2 s^{-1}$ for the near-red emission and 270 $\mu m^2 s^{-1}$ for the far-red emission. This again supports the conclusion that the near red impurity is not an aggregate, since Alexa 647 and the green fluorescent moiety have roughly the same hydrodynamic radius.

These studies indicate that Alexa 647 and Cy5 are potential sources of significant cross-talk when used together with organic Alexa 532 or Cy3 fluorophores with 532 nm excitation, or when used in conjunction with less intense protein based fluorophores excited with 561 nm light. We do not expect that the near-red fluorescence would be problematic in traditional single-molecule measurements, since the relative concentration of near-red-to-far-red fluorophore is low. However, this near-red fluorescence could lead to substantial artifacts in multicolor super-resolution experiments since Cy5 or Alexa 647 fluorophores are densely labeled, with most dyes residing in a reversible dark state for the majority of the measurement. Since the near-red moiety does not photoswitch, a significant number of fluorophores can be visualized at any given time. This is expected to only lead to minor artifacts in chemically fixed cells, since fluorescence signals that do not vary with time are typically removed in image processing. Aberrant signals could still subtly contaminate images if there is significant stage drift or if the excitation intensity is not stable with time. The presence of the near-red fluorescence more significantly complicates measurements when probes are mobile, as is the case when imaging membrane proteins within live cells. Under these conditions, background subtraction does not remove long-lived near-red fluorescence as these probes can explore large areas over a given measurement.

Multicolor super-resolution imaging in live cells has been accomplished previously by a large number of different groups,[20–30] and in most cases this impurity could not have impacted stated results. Our findings have no bearing on studies that exclusively used fluorescent proteins,[11,14,20–23] or proteins in combination with quantum dots,[24] since these probes are not investigated here. As far as we are aware, existing studies using mEos2 or mEos3.2 proteins in live cells in combination with organic fluorophores have not utilized Cy5 or Alexa 647, and instead have used Atto 655,[25,26] which we observe to be free of this fluorescent impurity. Past studies have also used other organic probe pairs in live cells, such as cationic rosamine and boron-dipyrromethene (BODIPY) dyes[27] or Alexa 488 in combination with Alexa 555.[28] Again, we do not expect that these probe pairs would lead to anomalous results based on our measurements. Several past studies have used Alexa 647 or Cy5 in combination with near-red dyes in live cells. In one, Alexa 647 was used in conjunction with Alexa 568 which is excited at 561 nm.[29] We do not anticipate that this near-red fluorescence would lead to anomalies in this measurement since single molecule event intensities of Alexa 568 should be orders of magnitude larger than the impurity and would be removed in image processing. At least one past study has used Cy3 and Cy5 in combination for live-cell super-resolution imaging.[30] It is possible that aspects of their results could be impacted by our observations, although we have not investigated the tetrazene or azide modified dyes used in this work.

In our own past work, we have imaged mEos3.2 in combination with Alexa 647 in chemically fixed cells,[31] and the small number of anomalous near-red fluorophores present in these samples did not impact our results. We only anticipate the results in fixed cells to be adversely affected when imaging Alexa 647 or Cy5 labelled species present at high local density in combination with a near-red labelled species present at low local density, especially when probes are anti-correlated.[32] In this case, an impurity present even at low mol% could adversely impact experimental results for fixed cells.

For multicolor live-cell measurements using Alexa532, mEos3.2, or mEos2, we recommend imaging these near-red probes in combination with a far-red probe such as Atto655 or Dyomics 654 to minimize possible artifacts. In principle, it should be possible to use chromatography techniques to separate the far-red Alexa 647 or Cy5 from the near-red dye prior to conjugation to protein. This purification is technically challenging due to the low concentration of near-red species, the hydrolysis of reactive groups on the dye, and the similarity in size between the two species. The photophysical properties of

Dy654 and Atto 655 are suitable for (d)STORM; however, the duty cycle of Dy654 and the photon yield of Atto 655 are less desirable than those of Alexa 647 and Cy5.[3] Overall, these experiments reinforce the need for careful controls in quantitative multicolor imaging measurements.

Supporting Information: Three movies containing simultaneous dual-excitation (647 and 561 nm) STORM raw data are available. All movies are time-lapse images acquired at 20 frames per second and displayed at 15 frames per second. The top panel of the movies shows far-red emission (660–740 nm) and the bottom panel near-red emission (576–630 nm). Movie S1, "BCR Alexa 647; Stone, Veatch.avi," contains images of Alexa 647 conjugated to $f(Ab)_1$ anti-mouse IgM labeling B cell receptor in live CH27 cells at room temperature. Movie S2, "Ctxb Alexa 647; Stone, Veatch.avi," contains images of Alexa 647 conjugated to cholera toxin subunit b labeling ganglioside GM1 in live CH27 cells at room temperature. Movie S3, "DiD(C18); Stone, Veatch.avi," contains images of diphytanoylphosphocholine lipid bilayers labeled with DiD-C18 at room temperature. Movie S4, "BCR Atto 655; Stone, Veatch.avi," contains images of Atto 655 conjugated to $f(Ab)_1$ anti-mouse IgM labeling B cell receptor in live CH27 cells at room temperature.

Experimental Section

Fluorescence Labeling

$f(Ab)_1$ goat antibody fragment to mouse IgM, μ chain specific (Jackson Immuno Research), was chemically modified with either Alexa Fluor 532 carboxylic acid succinimidyl ester, Alexa Fluor 647 carboxylic acid succinimidyl ester (Life Technologies), Atto 655 NHS ester (Sigma), or Dyomics-654-NHS-ester (Dyomics GmbH). Modifications were carried out in aqueous solution buffered by 0.01 M NaH_2PO_4 with 0.01 M NaH_2CO_3, pH 8.2 for one hour at room temperature. Reaction was quenched with addition of 10 mM 2-mercaptoethanol (Sigma) prior to gel filtration on illustra NAP-5 columns (GE Healthcare) to remove unbound dye from labeled protein. Typically each $f(Ab)_1$ is labeled with four dye molecules. Cy5 modified goat antibody to mouse IgM, μ chain specific, was purchased already conjugated to Cy5 (Jackson Immuno Research). Cholera toxin B subunit (Life Technologies) was purchased conjugated to Alexa Fluor 647. Glass-supported multilayers containing DiD-C_{18}, (dioctadecyl tetramethylindodicarbocyanine) (Invitrogen) and diphytanoylphosphocholine (Avanti Polar Lipids) were prepared by spin-coating lipids from chloroform, drying under vacuum, and hydrating with purified water.

Cells

CH27 cells were maintained in low-glucose Dulbecco's modified eagle's medium (DMEM, Gibco) containing 15% FBS (fetal bovine serum, Mediatech), 10 mM 4-(2-hydroxyethyl)-1-piperazineethanesulfonic acid (HEPES), 110 mg L^{-1} sodium pyruvate, 50 μM 2-mercaptoethanol (BME), and 1% Pen/Strep in 5% CO_2 at 37 °C. Cells were plated at 100 000 mL^{-1} and grown overnight on glass bottom wells (MatTek Corporation) before staining with 5 μg mL^{-1} labeled $f(Ab)_1$ for ten minutes and extensive washing with PBS prior to imaging. mEos3.2[16] tagged Lyn protein was created using standard cloning techniques from Lyn-eYFP[33] (a gift from Barbara Baird) and mEos3.2 was generated from mEos2[15] and was a kind gift from Akira Ono. 10^6 CH27 cells were transfected with 1 μg mEos3.2 tagged Lyn plasmid DNA (a gift from Akira Ono) in Clontech N1 vector (Clontech) using Lonza Nucleofector electroporation (Lonza) for expression of Lyn-mEos3.2 in Figure 1c.

Total Internal Reflection Fluorescence (TIRF) Microscopy

Imaging was performed on an Olympus IX81-XDC inverted microscope with a cellTIRF module, a 100X UAPO TIRF objective (NA = 1.49), active Z-drift correction (ZDC) (Olympus America). Images were acquired at 20 frames per second on an iXon-897 EMCCD camera (Andor). Excitation of fluorophores was accomplished using a 640 nm diode laser (CUBE 640-75FP, Coherent), a 561 nm optically pumped semiconductor laser (Sapphire 561-150 CW, Coherent), and a 532 nm diode-pumped solid-state laser (Samba 532-150 CW). Photoactivation of mEos3.2 was accomplished with a 405 nm diode laser (CUBE 405-50FP, Coherent). The laser energy density at sample is estimated to be 3 (561 nm), 14 (640 nm), and 20 kW cm^{-2} (530 nm). Excitation and emission was filtered using the quadband dichroic mirror LF405/488/561/635-4X-A-000 for 561 nm excitation, or LF405/488/561/635-4X-A-000 for 532 nm excitation (Semrock). Emission was split into two channels using a DV2 emission splitting system (Photometrics) with a T640lpxr dichroic mirror to separate emission, ET605/52m to filter near-red emission, and ET700/75m to filter far-red emission (Chroma). Samples were imaged in a buffer containing: 30 mM Tris, 100 mM NaCl, 5 mM KCl, 1 mM $MgCl_2$, 1.8 mM $CaCl_2$, 50 mM glucose, 12 mM glutathione, 40 μg mL^{-1} catylase, and 500 μg mL^{-1} glucose oxidase.

Single-Molecule Analysis

Single-molecule fluorescent events were determined by first finding local maxima with intensity greater than 5-sigma above fluctuations in background-subtracted images, then fitting background subtracted events to Gaussian functions using nonlinear least squares. The ensemble of events was then culled to remove outliers in brightness, size, and localization error.[12] Spatial registration of emission channels was accomplished using a method adapted from Churchman et al.[6] All data from event intensity analysis were taken with equivalent gain and excitation brightness, and were normalized by acquisition time to give intensity per second. Event intensity is determined by integrating the background subtracted intensity around the center of single molecule localizations with a radius of 560 nm, and intensity per unity time is determined by dividing this intensity by the camera integration time. Microscopy was controlled such that all acquisitions performed at a particular excitation wavelength used the same laser intensity, camera integration time, and gain settings. Super-resolution images were reconstructed by incrementing the intensity of pixels at positions corresponding to localized single molecules after correcting for stage drift and chromatic abberation.[6] All analyses were carried out in MATLAB (The MathWorks).

Fluorescence and Absorbance Spectroscopy

Fluorescence excitation and emission spectra were collected using an FP-6500 spectrofluorometer (Jasco) with a 150 W xenon lamp as excitation source and a 3 nm bandpass filter for excitation and emission. All fluorescence samples were measured in 4 mm pathlength quartz cuvettes (Starna). Fluorescence spectra from Alexa Fluor 647 carboxylic acid succinimidyl ester (Invitrogen), Cy5 Maleimide (GE Healthcare), Dyomics-654-NHS-ester (Dyomics), and Atto 655 NHS ester (Sigma) were acquired in Figure 3b. Absorbance

spectra were collected with a NanoDrop 2000 spectrophotometer (Thermo).

Fluorescence Correlation Spectroscopy

Fluorescence correlation spectroscopy was performed on an Olympus IX-81 microscope equipped with an ALBA dual-channel spectrophotometer (ISS) and a U Plan S-APO 60X 1.2 NA water immersion objective (Olympus America). Samples were excited with a WhiteLase Supercontinuum Source SC400-6-PP (Fianium), and excitation wavelengths were selected using an acousto–optic tunable filter (AOTF, Fianium). Excitation and emission were filtered using the quadband dichroic mirror 405/488/532/635 (Alluxa). Fluorescence signals passing through a 50 μm diameter pinhole were detected with an avalanche photodiode SPCM-AQRH-15 (PerkinElmer) and time-correlated single photon counting was accomplished using an SPCM-830 TCSPC module with a maximum 8 MHz detector count rate (Becker-Hickl GmbH). Instrumentation was controlled and data was analyzed using the VistaVision software (ISS). Time-averaged correlation functions from dye diffusion through excitation volume were fit to the model for three-dimensional motion, where N is the mean number of fluorescent molecules in the excitation volume, t is the time lag of the fluorescence correlation, t_D is the characteristic dwell time for a particular molecule and excitation volume, and k is a factor to account for the shape of the excitation volume [Eq. (1)]:

$$G(t) = \frac{1}{\left(N\left(1+\frac{t}{t_D}\right)\right)}\frac{1}{\sqrt{1+\left(\frac{t}{kt_D}\right)}} \quad (1)$$

This parameters N and t_D of Equation (1) were fit to $G(t)$, the experimentally determined time correlation function. The diffusion coefficient, D, was calculated using Equation (2), where w_{xy} is the beam waist of the focal volume in the xy plane:

$$D = \frac{w_{xy}^2}{4t_D} \quad (2)$$

w_{xy} was calibrated using the far-red emission of Cy5 and the near-red emission of Cy3 using published diffusion coefficients, that is, 250 $um^2 s^{-1}$ for Cy5[34] and 280 $um^2 s^{-1}$ for Cy3.[35] The three-dimensional excitation volume (V_{EX}) was calibrated using known concentrations, C_{dye}, of the control dyes, Cy3 and Cy5, in conjunction with the fit parameter N [Eq. (3)]:

$$V_{EX} = N/C_{dye} \quad (3)$$

V_{EX} for 630 nm excitation was 2.33 μm^3, whereas V_{EX} for 530 nm excitation was 3.87 μm^3.

Alexa 647 FCS curves were fit to Equation (1) to obtain N and converted to a concentration using the calibrated excitation volume for each channel. Different dilutions of Alexa 647 ($C_{dilution}$) were used to determine the concentration of the near-red and far-red species (C_{FCS}), as indicated in Table 1. C_{FCS} and $C_{dilution}$ are measured independently but are in good agreement for the far-red excitation of Alexa 647. Results in Figure 5 and Table 1, derived from a single experiment, are representative of two additional measurements.

Acknowledgements

We thank N. Gupta for supplying CH27 cells; K. Gurunathan and the University of Michigan SMART center for assistance with FCS experiments; A. Gafni, J. Schauerte, and C. Chang for assistance with bulk fluorescence measurements; and J. Ogilve, J. Biteen, and W. Cheng for helpful discussions. S. Veatch acknowledges support from the National Institute of Health (R00GM087810) and startup funds from the University of Michigan.

Keywords: fluorescence · fluorescent probes · live cells · quantitative imaging · super-resolution imaging

[1] M. Heilemann, E. Margeat, R. Kasper, M. Sauer, P. Tinnefeld, *J. Am. Chem. Soc.* **2005**, *127*, 3801 – 3806.
[2] T. Ha, P. Tinnefeld, *Annu. Rev. Phys. Chem.* **2012**, *63*, 595 – 617.
[3] G. T. Dempsey, J. C. Vaughan, K. H. Chen, M. Bates, X. Zhuang, *Nat. Methods* **2011**, *8*, 1027 – 1036.
[4] G. T. Dempsey, M. Bates, W. E. Kowtoniuk, D. R. Liu, R. Y. Tsien, X. Zhuang, *J. Am. Chem. Soc.* **2009**, *131*, 18192 – 18193.
[5] H. Bock, C. Geisler, C. A. Wurm, C. von Middendorff, S. Jakobs, A. Schönle, A. Egner, S. W. Hell, C. Eggeling, *Appl. Phys. B* **2007**, *88*, 161 – 165.
[6] L. S. Churchman, Z. Ökten, R. S. Rock, J. F. Dawson, J. A. Spudich, *Proc. Natl. Acad. Sci. USA* **2005**, *102*, 1419 – 1423.
[7] H. Shroff, C. G. Galbraith, J. A. Galbraith, H. White, J. Gillette, S. Olenych, M. W. Davidson, E. Betzig, *Proc. Natl. Acad. Sci. USA* **2007**, *104*, 20308 – 20313.
[8] F. V. Subach, G. H. Patterson, S. Manley, J. M. Gillette, J. Lippincott-Schwartz, V. V. Verkhusha, *Nat. Methods* **2009**, *6*, 153 – 159.
[9] G. Patterson, M. Davidson, S. Manley, J. Lippincott-Schwartz, *Annu. Rev. Phys. Chem.* **2010**, *61*, 345 – 367.
[10] M. Bates, B. Huang, G. T. Dempsey, X. Zhuang, *Science* **2007**, *317*, 1749 – 1753.
[11] S. Semrau, L. Holtzer, M. González-Gaitán, T. Schmidt, *Biophys. J.* **2011**, *100*, 1810 – 1818.
[12] S. L. Veatch, B. B. Machta, S. A. Shelby, E. N. Chiang, D. A. Holowka, B. A. Baird, *PloS One* **2012**, *7*, e31457.
[13] T. Toplak, E. Pandzic, L. Chen, M. Vicente-Manzanares, A. R. Horwitz, P. W. Wiseman, *Biophys. J.* **2012**, *103*, 1672 – 1682.
[14] A. Dupont, K. Stirnnagel, D. Lindemann, D. C. Lamb, *Biophys. J.* **2013**, *104*, 2373 – 2382.
[15] S. A. McKinney, C. S. Murphy, K. L. Hazelwood, M. W. Davidson, L. L. Looger, *Nat. Methods* **2009**, *6*, 131 – 133.
[16] M. Zhang, H. Chang, Y. Zhang, J. Yu, L. Wu, W. Ji, J. Chen, B. Liu, J. Lu, Y. Liu, et al., *Nat. Methods* **2012**, *9*, 727 – 729.
[17] A. K. Chibisov, G. V. Zakharova, H. Görner, *Phys. Chem. Chem. Phys.* **2001**, *3*, 44 – 49.
[18] H. J. Gruber, C. D. Hahn, G. Kada, C. K. Riener, G. S. Harms, W. Ahrer, T. G. Dax, H. G. Knaus, *Bioconjugate Chem.* **2000**, *11*, 696 – 704.
[19] J. E. Berlier, A. Rothe, G. Buller, J. Bradford, D. R. Gray, B. J. Filanoski, W. G. Telford, S. Yue, J. Liu, C.-Y. Cheung, et al., *J. Histochem. Cytochem.* **2003**, *51*, 1699 – 1712.
[20] F. V. Subach, G. H. Patterson, M. Renz, J. Lippincott-Schwartz, V. V. Verkhusha, *J. Am. Chem. Soc.* **2010**, *132*, 6481 – 6491.
[21] J. C. M. Gebhardt, D. M. Suter, R. Roy, Z. W. Zhao, A. R. Chapman, S. Basu, T. Maniatis, X. S. Xie, *Nat. Methods* **2013**, *10*, 421 – 426.
[22] A. Gahlmann, J. L. Ptacin, G. Grover, S. Quirin, A. R. S. von Diezmann, M. K. Lee, M. P. Backlund, L. Shapiro, R. Piestun, W. E. Moerner, *Nano Lett.* **2013**, *13*, 987 – 993.
[23] M. S. Gunewardene, F. V. Subach, T. J. Gould, G. P. Penoncello, M. V. Gudheti, V. V. Verkhusha, S. T. Hess, *Biophys. J.* **2011**, *101*, 1522 – 1528.
[24] I. Izeddin, C. G. Specht, M. Lelek, X. Darzacq, A. Triller, C. Zimmer, M. Dahan, *PloS One* **2011**, *6*, e15611.
[25] S. Wilmes, M. Staufenbiel, D. Lisse, C. P. Richter, O. Beutel, K. B. Busch, S. T. Hess, J. Piehler, *Angew. Chem.* **2012**, *124*, 4952 – 4955; *Angew. Chem. Int. Ed.* **2012**, *51*, 4868 – 4871.
[26] U. Endesfelder, S. Malkusch, B. Flottmann, J. Mondry, P. Liguzinski, P. J. Verveer, M. Heilemann, *Molecules* **2011**, *16*, 3106 – 3118.
[27] S.-H. Shim, C. Xia, G. Zhong, H. P. Babcock, J. C. Vaughan, B. Huang, X. Wang, C. Xu, G.-Q. Bi, X. Zhuang, *Proc. Natl. Acad. Sci. USA* **2012**, ##DOI: 10.1073/pnas.1201882109.

[28] V. Mennella, B. Keszthelyi, K. L. McDonald, B. Chhun, F. Kan, G. C. Rogers, B. Huang, D. A. Agard, *Nat. Cell Biol.* **2012**, *14*, 1159 – 1168.
[29] S. A. Jones, S.-H. Shim, J. He, X. Zhuang, *Nat. Methods* **2011**, *8*, 499 – 505.
[30] I. Nikić, T. Plass, O. Schraidt, J. Szymański, J. A. G. Briggs, C. Schultz, E. A. Lemke, *Angew. Chem.* **2014**, *126*, 2278 – 2282; *Angew. Chem. Int. Ed.* **2014**, *53*, 2245 – 2249.
[31] J. R. Grover, G. N. Llewellyn, F. Soheilian, K. Nagashima, S. L. Veatch, A. Ono, *J. Virol.* **2013**, JVI.03526-12.
[32] D. Kim, N. M. Curthoys, M. T. Parent, S. T. Hess, *J. Opt.* **2013**, *15*, 094011.
[33] P. S. Pyenta, D. Holowka, B. Baird, *Biophys. J.* **2001**, *80*, 2120 – 2132.
[34] J. Widengren, P. Schwille, *J. Phys. Chem. A* **2000**, *104*, 6416 – 6428.
[35] H. S. Muddana, T. T. Morgan, J. H. Adair, P. J. Butler, *Nano Lett.* **2009**, *9*, 1559 – 1566.

Received: February 3, 2014
Revised: March 6, 2014
Published online on April 29, 2014